Optics Communications 426 (2018) 41–45

Contents lists available at ScienceDirect

Optics Communications

journal homepage: www.elsevier.com/locate/optcom

Electromagnetic exploration of focusing properties of high-numerical-aperture micro-Fresnel zone plates

Suqin Xue [a], Qiang Liu [b], Tao Liu [b,*], Shuming Yang [b], Pengfei Su [a], Kang Liu [b], Bo Tian [b], Tong Wang [b]

[a] Yan'an University, Yan'an 716000, China
[b] State Key Laboratory for Manufacturing Systems Engineering, Xi'an Jiaotong University, Xi'an 710049, China

ARTICLE INFO

Keywords:
Diffraction
Subwavelength structures
Zone plate
Binary optics
Polarization

ABSTRACT

Focusing properties of high-numerical-aperture micro-Fresnel zone plates (FZP) have been rigorously investigated at the wavelength from deep ultraviolet to visible based on the combination of the vectorial angular spectrum theory and three-dimensional finite-difference time-domain method. New insights are found. The axial spot size evaluated by full-width-at-half-maximum is in direct proportion to the inverse of the total annulus number. Linearly negative focal shift phenomenon can be observed due to the wavelength dispersion over a finite range of tens of nanometers. A proper wavelength deviation can lead to the maximum focal intensity. A simple method has been demonstrated to probe either multi-focus or a light needle using a composite microstructure based on high-NA FZPs. The findings of this study expand the common understandings of the classic widely-used FZPs.

1. Introduction

Fresnel zone plate (FZP) suits a variety of applications, e.g. in atomic optics, confocal imaging, and X-ray nanoscopy [1–3]. Recently, wide attention has been paid on super-focusing and nano-imaging of micro-Fresnel zone plates [4–8]. The focusing performance for a high-NA (numerical aperture) FZP is quite different from the well-known situation for a very low-NA FZP (multi-focus). One fact is that there is one single main focus for a relatively high-NA FZP [6,7,9].

Thus far, there are still three main problems unresolved for high-NA micro-FZPs. First, the vectorial nature of the incident light source must be considered, which requires to use one suitable vectorial diffraction theory instead of the simplified scalar diffraction theories, e.g. Fresnel–Kirchhoff diffraction integral. Second, a micro-FZP is comprised of micro-annuli, which are at the subwavelength scale. The polarization-dependent transmission effect may become pronounced, especially when the maximum focusing angle dramatically increases (high NA) [10,11]. This situation needs to be examined by a rigorous electromagnetic simulation method. Third, the fabrication of a FZP is based on the design (or ideal) wavelength (λ_0) and the illumination wavelength (λ_i) usually equals to the design wavelength. So, most previous researches have mainly concentrated on FZPs under the assumption of $\lambda_i = \lambda_0$. In practice, λ_i may largely deviate from λ_0 ($\lambda_i \neq \lambda_0$). The chromatic dispersion effect has to be particularly studied. In the above situations, novel focusing properties are to be disclosed.

In this paper, vectorial angular spectrum (VAS) theory has been elected as the theoretical basis [12,13]. The numerical results will be compared with the rigorous results given by the three-dimensional finite-difference time-domain (FDTD) method. This study will significantly expand the common understandings of classic widely-used FZPs. Potential applications can be found. For example, the super-focusing performance for a high-NA FZP can be used in high-resolution laser scanning confocal microscopy by replacing the bulky, costly objective lens with a planar, light-weight FZP. It is also useful in laser microfabrication if a pulsed femto-second laser is used. The linear focal shift phenomenon can be applied to implement the axial wavelength scanning in chromatic confocal microscopy and particle manipulation.

2. Methods

2.1. Vectorial angular spectrum representation

For a binary FZP, the radius coordinates of each annulus are determined by $r_n = (n\lambda f + n^2\lambda^2/4)^{1/2}$, $n = 0, 1, 2, \ldots, N$ [6,7,9]. f is the main focal length and N is the total annulus number. λ is the light

* Corresponding author.
E-mail address: liu8483@xjtu.edu.cn (T. Liu).

https://doi.org/10.1016/j.optcom.2018.05.014
Received 12 March 2018; Received in revised form 18 April 2018; Accepted 6 May 2018

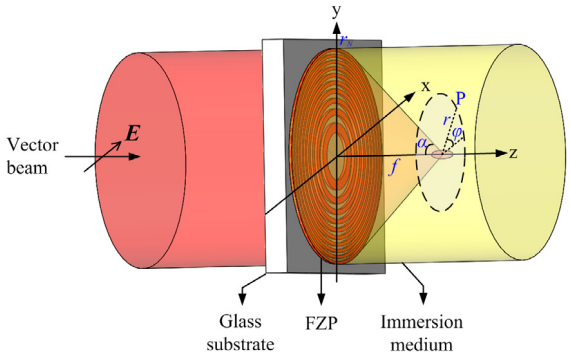

Fig. 1. Schematic diagram of focusing a linearly polarized vector beam by a high-NA immersed FZP.

wavelength in the medium where the FZP is immersed. $\lambda = \lambda_0/\eta$ with λ_0 being the illumination light wavelength and η the refractive index of the immersion medium, as shown in Fig. 1. The equivalent numerical aperture (NA) of a FZP is still defined by $\mathrm{NA} = \eta \sin\alpha$, similar to the case for a traditional objective lens [4,7,9,13]. α is the maximum focusing semi-angle, satisfying $\tan\alpha = r_N/f$. The diameter of a FZP is $D = 2r_N$.

For a binary amplitude-type FZP, the transmission function $t(r)$ is mathematically described as

$$t(r) = \begin{cases} 1, & r_{2m} < r \le r_{2m+1} \\ 0, & r_{2m+1} < r \le r_{2m+2} \end{cases}, \tag{1}$$

where, $m = 0, 1, \ldots, N/2-1$ and N is supposed to be an even number here. In Eq. (1), the innermost circle is assumed to be transparent.

For a linearly polarized beam (LPB, polarized along x direction) normally illuminating a FZP, as shown in Fig. 1, components of the electric field $\boldsymbol{E}$ for any point P (r, φ, z) in the observation plane $(z>0)$ are derived in our previous reports according to the VAS theory, as [12–15]

$$\begin{cases} E_x(r,z) = \int_0^\infty A_0(l)\exp\left[\mathrm{j}2\pi q(l)z\right] J_0(2\pi lr)2\pi l\mathrm{d}l \\ E_y(r,z) = 0 \\ E_z(r,\varphi,z) = -\mathrm{j}\cos\varphi \int_0^\infty \frac{l}{q(l)} A_0(l)\exp\left[\mathrm{j}2\pi q(l)z\right] J_1(2\pi lr)2\pi l\mathrm{d}l \end{cases}, \tag{2}$$

where, $q(l) = (1/\lambda^2 - l^2)^{1/2}$ and l is the radial spatial frequency component. J_0 and J_1 are the zeroth and first order Bessel functions of the first kind, respectively. $A_0(l)$ in Eq. (2) is

$$A_0(l) = \int_0^\infty t(r)g(r)J_0(2\pi lr)2\pi r\mathrm{d}r, \tag{3}$$

where, $t(r)$ is described by Eq. (1) representing the scalar transmission (polarization-insensitive) function for a FZP, which is a basic assumption (thin element approximation) [7,12,16]. $g(r)$ denotes the amplitude distribution of the illumination vector beam at the mask plane of FZP. $g(r) = 1$ for a uniform plane wave. The total electric energy density (or light intensity) is calculated by $I(r,\varphi,z) = |\boldsymbol{E}(r,\varphi,z)|^2 = |E_x(r,z)|^2 + |E_z(r,\varphi,z)|^2$.

2.2. FDTD simulation

The focusing process of a FZP can be divided into two steps: light transmitting microstructured annular grooves and light propagation in a homogeneous, dielectric medium (Fig. 1). If the electric field immediately behind FZP is known, the VAS theory is always valid for describing the light propagation which is complicated to be explicitly described. So assumptions have to be applied, which mostly uses a scalar function t and neglects the polarization-dependent transmission effect [7,8,11–16]. However, this assumption may induce slight errors [11] and thus the VAS-predicted results need to be physically examined by the 3D FDTD method, which numerically solving Maxwell's equations [17]. The total-field scattered-field (TFSF) boundary and perfectly matched layer (PML) absorbing boundary condition are used in the following FDTD simulations. For binary amplitude FZPs, it is crucial to properly select the type and thickness of the metallic film, which is coated on the glass substrate to attenuate the incident light. At the visible spectrum, a 100 nm-thick aluminum film is usually a good choice [14]. However, for the deep ultraviolet light (193 nm), it is found that a 25 nm-thick aluminum film is preferable [18].

3. Results

Full width at half maximum (FWHM) is used to evaluate the spot size in each direction. The illumination light source is typically a uniform plane beam (x-polarized LPB). The wavelength deviation of the illumination light (λ_i) is described by $\Delta\lambda_0$, denoted by $\lambda_i = \lambda_0 + \Delta\lambda_0$. Here $\lambda_0 = \eta\lambda$ is also termed as the design wavelength. In Table 1, typical wavelengths are selected from deep ultraviolet to visible. These wavelengths are common for widely-used lasers. The focal lengths are selected due to the computation resource of the workstation (RAM 128 GB) available.

3.1. Single focus and spot size

It is well-known that for a very-low NA FZP (NA<0.1), there will be multi-focus behind the FZP. The position and peak intensity for each secondary focus can be known from the main focus. Two groups of FZP ($\mathrm{FZP_{1G}}$ and $\mathrm{FZP_{2G}}$, Table 1) are used to explore the focusing properties for high-NA FZPs. For the first group ($\mathrm{FZP_{1G}}$), the main focal length f is 3 μm and the illumination wavelength λ_0 is 193 nm (deep ultra-violet laser). The total annulus number N is increasing from 4 to 150. The corresponding NA is hereby increasing from 0.571 to 1.401. This group of FZPs has been immersed in water. The refractive index is 1.44 for $\lambda_0 = 193$ nm [18]. The results have been compared in Fig. 2. It can be seen that the results calculated by VAS and FDTD are well agreed.

The multi-focus distribution disappears when N>10 (NA>0.83). A pure single focus appears. The axial position for the peak intensity of the focus is represented by z_p in Fig. 2(a). Thus, with NA increasing, the focal position remains almost unchanged. The peak intensity of the focus, denoted by I_p, is increasing and it dramatically grows for higher NAs, as shown in Fig. 2(b). The axial spot size, denoted by FWHM_z, is plotted in Fig. 2(c) with respect to NA. So, the focus will be compressed with the increasing of NA. Meanwhile, FWHM_z is replotted with respect to $1/N$ in Fig. 2(d). Obviously, the axial spot size is in direct proportion to the inverse of the total annulus number, which can be expressed by $\mathrm{FWHM}_z \propto 1/N$. It should be indicated that there exists a theoretical limit of about $0.9\lambda_0/\eta$ which can be inferred from Eq. (7) in Ref. [9]. For example, if $f = 5$ μm, $\lambda_0 = 633$ nm, $N = 400$, then $\mathrm{NA} = 0.9993$. FWHM_z is calculated to be 0.64 μm ($1.01\lambda_0$) according to the VAS theory. The transverse spot sizes at $z = f$ are compared in Fig. 2(e). For a lens optical system, Abbe's diffraction resolution limit is calculated by $\lambda_0/(2\mathrm{NA})$, which is also plotted (red dashed line). The spot size in y direction is decreasing with NA and surpasses the diffraction limit when NA>1. The reason for super-focusing can be explained using the apodization factor. The apodization factor is $\cos^{1/2}\theta$ [19] and $\cos^{-3/2}\theta$ [4] for the lens and FZP systems, respectively. For $\mathrm{NA} = 1.4$, $\mathrm{FWHM}_y = 59$ nm ($0.3\lambda_0$). However, in x direction, the spot size is first decreasing and then slightly increasing when NA>1.2. For the very high NA, the transverse spot takes a dumbbell shape and it is no longer circular. This can be explained from Eq. (2). The reason is the longitudinally polarized component E_z is noncircular. It vanishes along y direction ($\varphi = \pi/2$). This phenomenon is trivial for high-NA focusing elements, e.g. refractive lens-based objectives. The focal spot for a high-NA FZP has no pronounced side lobes. The light efficiency can be simply evaluated by the ratio of the transparent area to the overall illuminated area. For $\mathrm{FZP_{1G}}$, it is increasing from 49.5% to 49.8% when N is increasing from 4 to 150.